Self-Supervised Vision Transformers Learn Visual Concepts in Histopathology

Richard J. Chen[*]
Department of Biomedical Informatics
Department of Pathology
Harvard Medical School

Rahul G. Krishnan[*]
Department of Computer Science
Department of Laboratory Medicine and Pathobiology
University of Toronto

Abstract

Tissue phenotyping is a fundamental task in learning objective characterizations of histopathologic biomarkers within the tumor-immune microenvironment in cancer pathology. However, whole-slide imaging (WSI) is a complex computer vision in which: 1) WSIs have enormous image resolutions with precludes large-scale pixel-level efforts in data curation, and 2) diversity of morphological phenotypes results in inter- and intra-observer variability in tissue labeling. To address these limitations, current efforts have proposed using pretrained image encoders (transfer learning from ImageNet, self-supervised pretraining) in extracting morphological features from pathology, but have not been extensively validated. In this work, we conduct a search for good representations in pathology by training a variety of self-supervised models with validation on a variety of weakly-supervised and patch-level tasks. Our key finding is in discovering that Vision Transformers using DINO-based knowledge distillation are able to learn data-efficient and interpretable features in histology images wherein the different attention heads learn distinct morphological phenotypes. We make evaluation code and pretrained weights publicly-available at: https://github.com/Richarizardd/Self-Supervised-ViT-Path.

1 Introduction

Tissue phenotyping is a fundamental problem in computational pathology that aims at learning objective characterizations of histopathologic biomarkers within the tumor-immune microenvironment for cancer diagnosis, prognosis, and response-to-treatment [1, 2, 3]. In cancer pathology, the current clinical paradigm is the manual and subjective interpretation of histology whole-slide images (WSI) in determining clinical endpoints such as cancer subtype, grade, and stage [4]. Though used as the gold standard in taxonomic classifications and staging systems for many cancer types, such subjective interpretation has been demonstrated to suffer from large inter- and intra-observer variability [5, 6]. For instance, the substantial variability in discerning well-to-poorly differentiated glands in the Gleason grading system for prostate adenocarcinoma, or the evaluation of nuclear size, shape, and nucleolar prominence in the Furhman grading system for renal cell carcinoma [7, 8]. Though current efforts using deep learning have progressed the field towards using Convolutional Neural Networks (CNNs) with pixel-level annotations, the large image resolutions of WSIs add cost to annotation workflows and precludes the development of tissue phenotyping algorithms at scale in addressing diverse tasks.

To address the limitations of using pixel-level annotations for tissue phenotyping, recent progress in set-based deep learning have adopted frameworks such as multiple instance learning (MIL) for weak-supervision of WSIs using only slide- or patient-level labels. Such frameworks follow two steps: 1) instance-level patch embeddings are extracted from non-overlapping tissue patches in the

---

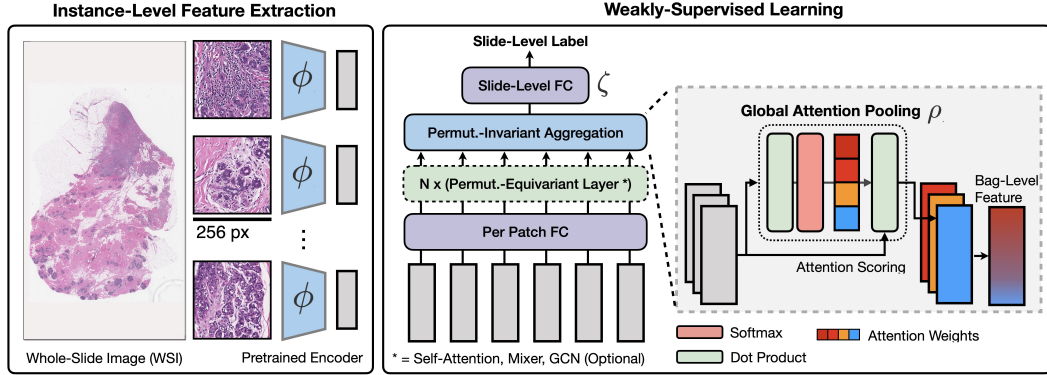[*] Part of this work performed while at Microsoft Research New England.

Figure 1: Conventional weak-supervision in WSIs using multiple instance learning and set-based deep learning. Feature embeddings are extracted using an encoding function ϕ (pretrained ResNet50 on ImageNet after the 3rd residual block), with only ρ, ψ trained in feature aggregation (ρ typically implemented as global attention pooling from Ilse *et al.*. Permutation-equivariant functions (*e.g.* - MLP-Mixer, Transformer attention, graph convolutions) can be optionally stacked before pooling) [12, 13, 15].

WSI, and then 2) global pooling is applied over the bag to construct a WSI-level embedding [9]. This work studies the first of those two steps in building predictive models from histopathological images. In the status quo, there is a lack of diverse and well-curated pathology datasets that would enable generalization across diverse tissue and organ types in cancer pathology. Consequently, a common choice made for the instance-level feature extractor is a ResNet-50 encoder pretrained on the ImageNet dataset. Although a reasonable starting point, this model which may not capture all the domain-specific features relevant in downstream tasks for cancer pathology [11] due to the differences between histopathological images and natural images.

More recently, deep learning has witnessed a surge in self-supervised learning [16, 17, 18, 19, 20, 21, 22] as a paradigm for learning feature representations without the use of labels. Self-supervised learning leverages the insight that one can learn useful representations of high-dimensional data through the use of auxiliary tasks such as identifying that the representation of an image (under a information preserving transformation) should not change very much. While self-supervised learning has been proposed as a replacement for ResNet-50 encoders pretrained on ImageNet [23, 24] in pathology tasks, we note two limitations of existing work. The first is a lack of comprehensive benchmarks that evaluate self-supervised models on diverse patch-level and weakly-supervised tasks, and the second is a lack of introspection and post-hoc assessment of the learned self-supervised representations in understanding what morphological features are learned.

The overarching objective of this work is to learn good representations for WSIs and understand what aspects of histopathological images are captured by such representations. We highlight the following contributions of our work:

1. We train several state-of-the-art self-supervised learning models and apply them to a diverse variety of patch-level and weakly-supervised tissue phenotyping tasks in computational pathology. In doing so, we study how the inductive biases of these techniques affect the quality of representations in downstream tasks. Our benchmark evaluates two different self-supervised models (SimCLR, DINO) trained on the breast invasive carcinoma (BRCA) cohort in The Cancer Genome Atlas (TCGA).

2. We find from analysis of our baselines that ResNet-50 encoders pretrained on ImageNet work better than previously reported, achieving comparable performance to a several self-supervised pretraining methods.

3. Next, we show that self-supervised learning via knowledge distillation in DINO [22] achieves the highest performance across a majority of tasks. We believe that this improvement comes from potential local-global correspondences captured in DINO data augmentation, which may model part-whole hierarchies inherent in histopathology imaging data (*e.g.* - local image crops describing cells in the global tissue patch).

4. Finally, we find that DINO learn visual concepts of histopathology tissue in localizing stroma tissue, cell location, and regions of fat / air pockets with different attention heads, suggesting that ViTs are able to capture important inductive biases about histopathology tissue.

2   Related Work

Unsupervised Learning for Tissue Phenotyping. Recent work in unsupervised deep learning has focused on devising proxy objectives to train deep networks in the absence of target labels, demonstrating impressive performance on image representation learning on both natural images and histology tissue patches. Oord *et al.* proposed one of the first methods in self-supervised learning using contrastive losses (called Contrastive Predictive Coding, or CPC), which aims to maximize the mutual information between 64×64 image patches within a 256×256 image (positive target), and minimize the mutual information between image patches of different images in the mini-batch (negative target) [16]. Similarly, Chen *et al.* proposed a contrastive framework that maximizes the cosine similarity between two data-augmented views of the same image, and minimizes similarity between different images within the mini-batch [18]. In pathology applications, CPC, SimCLR, and other similar self-supervised methods have been used for cell- and tissue-level phenotyping, with downstream applications in cancer diagnosis, cancer prognosis, and gene mutation prediction [26, 27, 28, 29, 30, 31, 32, 33, 34, 29, 35]. However, an important limitation is that though achieving strong performance on standard benchmarks such as ImageNet and STL-10, these methods depend on strong assumptions about the class balance of the dataset, as sampled minibatches would typically sample images of different classes in these datasets. Such assumptions may not hold in WSIs, as depending on the cancer type, there may exist large class imbalances of morphological phenotypes as sampled histology patches may comprise of only one class and have similar statistical image properties (e.g. - only benign tissue) [36]. In addition to contrastive learning, self-supervised learning via student-teacher knowledge distillation frameworks have recently emerged in achieving state-of-the-art results on ImageNet Top-1 and Top-5 benchmarks [20, 22, 37]. An important distinction in comparison to contrastive learning is that these methods can be trained without the need of negative targets, however, large-scale efforts in benchmarking knowledge distillation self-supervision in computational pathology have had limited attention.

Weakly-Supervised Learning in WSIs. Remarkable progress have been made in weakly-supervised learning in WSIs using set-based network architectures. In general set-based deep learning, Edwards and Storkey and Zaheer *et al.* proposed the first network architectures operating on set-based data structures [38, 39]. In pathology, Ilse *et al.* extended set-based network architectures as an approach for multiple instance learning in histology region-of-interests, with Campanella *et al.* later extending end-to-end weak-supervision on gigapixel WSIs [40, 9]. Lu *et al.* demonstrated that by using a pretrained ResNet-50 encoder on ImageNet at the instance-level feature extraction step, only a global pooling operator needs to be trained in reaching state-of-the-art performance on many diagnostic subtyping tasks [11]. Following the work of Lu *et al.*, there have been many variations of MIL that have adapted unsupervised learning techniques such as VAE-GAN, SimCLR, and MOCO as instance-level feature extraction [28, 26, 30, 33]. However, we note that there is a lack of comprehensive benchmarks that evaluate self-supervised models on diverse patch- and slide-level tasks.

3   Background

Notation: For a given WSI, let $\mathbf{x}$ refer to a 256×256 tissue-containing image patch at $20\times$ magnification, with the bag of the M tissue-containing patches in the WSI as $\mathbf{X} = \{\mathbf{x}_1, \ldots, \mathbf{x}_M\} \in \mathbb{R}^{M \times 3 \times 256 \times 256}$. Let Y denote the slide-level label corresponding to $\mathbf{X}$, and y refer to the patch-level label corresponding to $\mathbf{x}$. We use $\phi : \mathbb{R}^{3 \times 256 \times 256} \to \mathbb{R}^{1 \times d}$ to denote an encoder that extracts d-dim features from $\mathbf{x}$. After applying ϕ per-patch we obtain a bag of extracted features $\mathbf{H} = \{\mathbf{h}_1, \ldots, \mathbf{h}_M\} \in \mathbb{R}^{M \times d}$.

Slide-Level Classification. Multiple Instance Learning (MIL) is a framework that operates on bags of embedding instances, in which label information is provided at the bag-level but not the instance-level. The primary goal is to solve the bag classification task $P(Y|\mathbf{X})$, with the additional challenge of discovering key instances $\mathbf{x}$ that would trigger the bag label. As a set-based network architecture,

we train a permutation-invariant function $\mathcal{F}$ that has the general form:

$$\mathcal{F}(X) = \zeta\big(\rho\left(\{\phi(\mathbf{x}_i) : \mathbf{x}_i \in \mathbf{X}\}\right)\big) \tag{1}$$

which learns: 1) the encoder ϕ applied instance-level extracting $\mathbf{h}$ from $\mathbf{x}$ in the bag, 2) the symmetric, permutation-invariant aggregation function $\rho : \mathbb{R}^{m \times d} \to \mathbb{R}^{1 \times d}$ that pools $\mathbf{h}$ in the bag as the bag-level feature $\mathbf{H}$, and 3) a bag-level classifier $\zeta : \mathbb{R}^d \to \mathbb{R}^{\# \text{class}}$ that further processes the bag-level features for downstream classification tasks. In current frameworks for MIL in WSIs, training $\mathcal{F}$ is usually not performed end-to-end due to computational complexity of gigapixel image resolutions. In Lu *et al.*, ϕ is implemented as a pretrained ResNet-50 model on ImageNet truncated after the 3rd residual block (denoted as ResNet-50-B3$_{\text{IN}}$) extracting 1024-dim features (**Figure 1**) [11]. As a result, only ρ, ζ are trained in MIL, typically parameterized using the global attention pooling function in Ilse *et al.* [40].

Patch-Level Classification: Using pixel-level annotations y, extracted feature embeddings using ϕ can then be finetuned for simple patch classification $P(y|\mathbf{x})$, in which ϕ is a previously pretrained ResNet-50 or ViT model. We note that though tissue phenotyping can be formulated as a segmentation problem, due to the gigapixel image resolutions of WSIs, patches contained within segmentation masks would typically belong to one class. For some tasks such as cell type classification in which patches can have an admixture of diverse phenotypes, we use the majority phenotype label as the patch label [41].

4 Self-Supervised learning as Instance-Level Pretraining

While using ResNet-50-B3$_{\text{IN}}$ as the instance-level feature extraction ϕ has been successful in many weakly-supervised tasks, the extracted feature embeddings from an out-of-domain classifier may not generalize well across phenotyping tasks in cancer pathology. In this work, we study several self-supervised methods to pretrain ϕ for downstream tasks, and explore the quality of representations of SimCLR and DINO. Moreover, we note several unique properties about DINO pretraining, which we note below in the application of image pretraining for pathology data.

SimCLR and DINO Overview: Self-supervised approaches work by taking an image $\mathbf{x}$, an augmented image $\tilde{\mathbf{x}}$ (where $\mathcal{T} : \mathbf{x} \to \tilde{\mathbf{x}}$ is an image transformation that preserves information content e.g. a slight rotation) and comparing the representations $\phi(\mathbf{x}), \phi(\tilde{\mathbf{x}})$ in different ways. SimCLR learns the representation ϕ by minimizing $\dfrac{\exp(\text{sim}[\phi(\mathbf{x}_i), \phi(\tilde{\mathbf{x}}_i)])}{\sum_k \exp(\text{sim}[\phi(\tilde{\mathbf{x}}_i), \phi(\mathbf{x}_k)])}$, where $\mathbf{x}_k = \{\mathbf{x}_j \neq \mathbf{x}_i; \mathbf{x}_j \in \mathbf{x}_{\text{minibatch}}\}$ and *sim* is a similarity function (e.g. the dot product between two vectors). For images in $\mathbf{x}_{\text{mini-batch}}$, the goal is to learn a representation that is robust to transformations that $\mathcal{T}$ that preserve the information content within the image, via maximizing similarity between data-augmented views of the same image (positive target) and minimizing similarity between views from different images in the mini-batch. As mentioned, however, this assumption may not hold for sampled mini-batches in pathology data which may have large class imbalance of represented morphological phenotypes. In DINO, rather than using a contrastive loss, student-teacher knowledge distillation is used, in which a student function ϕ_s is trained to match the probability distribution of a Siamese teacher network ϕ_t using the cross-entropy loss $-p_s(\mathbf{x}) \log p_t(\mathbf{x})$ with momentum encoding, with p_s, p_t denoting the outputs of $\phi_s(\mathbf{x}), \phi_t(\mathbf{x})$ respectively for image $\mathbf{x}$ (**Figure 2**) [22]. A desirable property of DINO in the application of self-supervised learning to pathology data is that negative targets are not needed to steer representation learning.

Different methods use different choices for $\mathcal{T}$. In SimCLR, color jittering, random crops and resizes, and horizontal flips used to augment the image while still preserving semantic information. DINO additionally constructs a set of 8 local views (96×96 crops, passed through ϕ_s) and 2 global views (224×224 crops, passed through ϕ_t) to encourage local-to-global correspondences between the student and teacher. An intriguing property that makes this data augmentation particularly well suited for histology data is the inherent part-whole hierarchy of cells in a tissue patch [42, 43, 44]. In comparison to natural images in which 96×96 crops may capture only colors and textures without any semantic information, at $20\times$, local 96×96 image patches encapsulate single cells and their surrounding extracellular matrices, which has shared mutual information with the broader spatial organization of cells in the global views.

Parameterizing ϕ: SimCLR uses a ResNet-50 encoder for ϕ. In contrast, DINO uses a Vision Transformer (ViT) as the image encoder. As input, 256×256 image patches are further tessellated
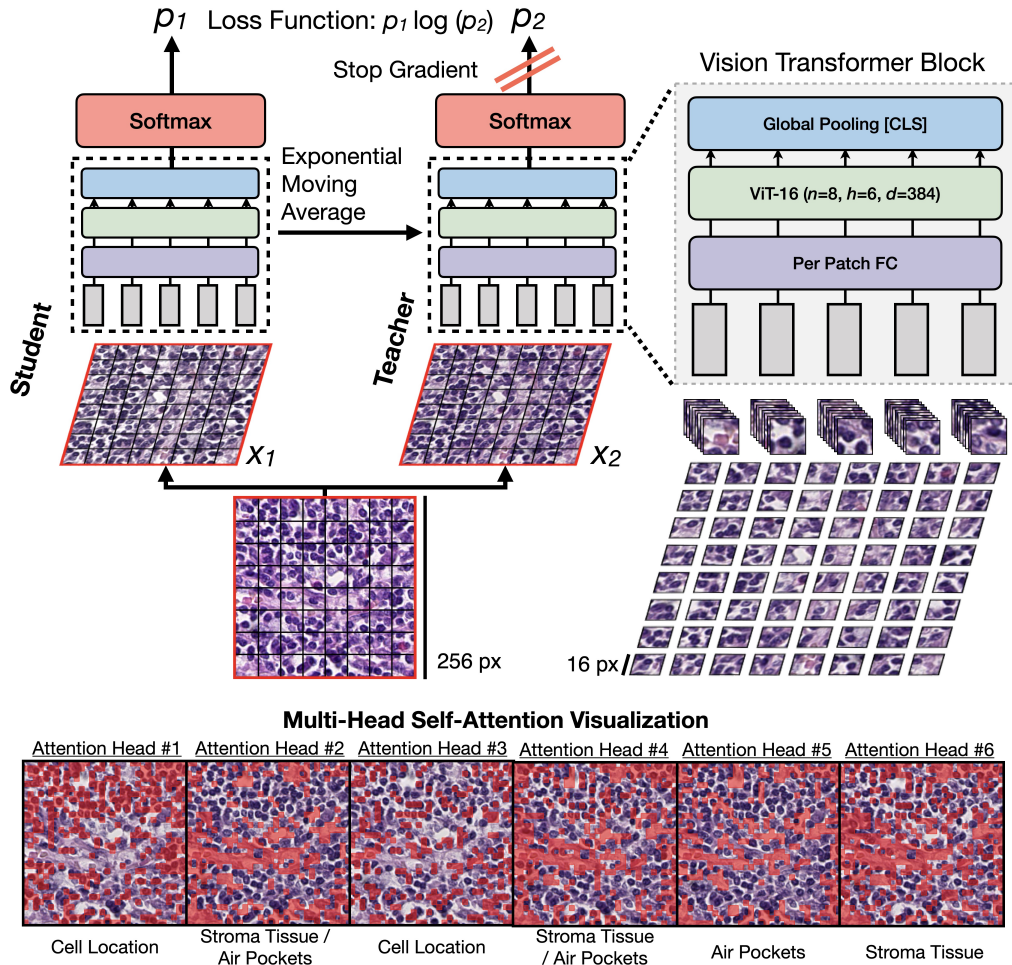
Figure 2: Self-supervision using knowledge distillation in DINO to pretrain ϕ on histology image patches [22]. A student network ϕ_s is trained to match the probability distribution of a Siamese teacher network ϕ_t using a cross-entropy loss, with ϕ parameterized using a Vision Transformer (ViT) model, and local and global crops applied as data augmentation. Interpretability of multi-head attention weights reveal that DINO learns distinct morphological phenotypes.

into non-overlapping 16×16 patches, with multi-head self-attention layers from Vaswani *et al.* used as permutation-equivariant feature aggregation functions to learn interactions between the smaller patches. This choice allows the model to learn how cells are organized in the tissue patch [13].

5   Experiments and Results

5.1   Training ϕ:

To create the training datasets for image pretraining, we used the Tissue Image Analysis (TIA) toolbox to tessellate each WSI into non-overlapping 256×256 tissue-containing patches at $20\times$ magnification. In total, 2055742 image patches were curated from 1038 WSIs from the TCGA-BRCA cohort. All methods were developed on the same training datasets (of each organ type) with standard learning and data augmentation parameters of their respective source papers, and evaluated at 100 epochs.
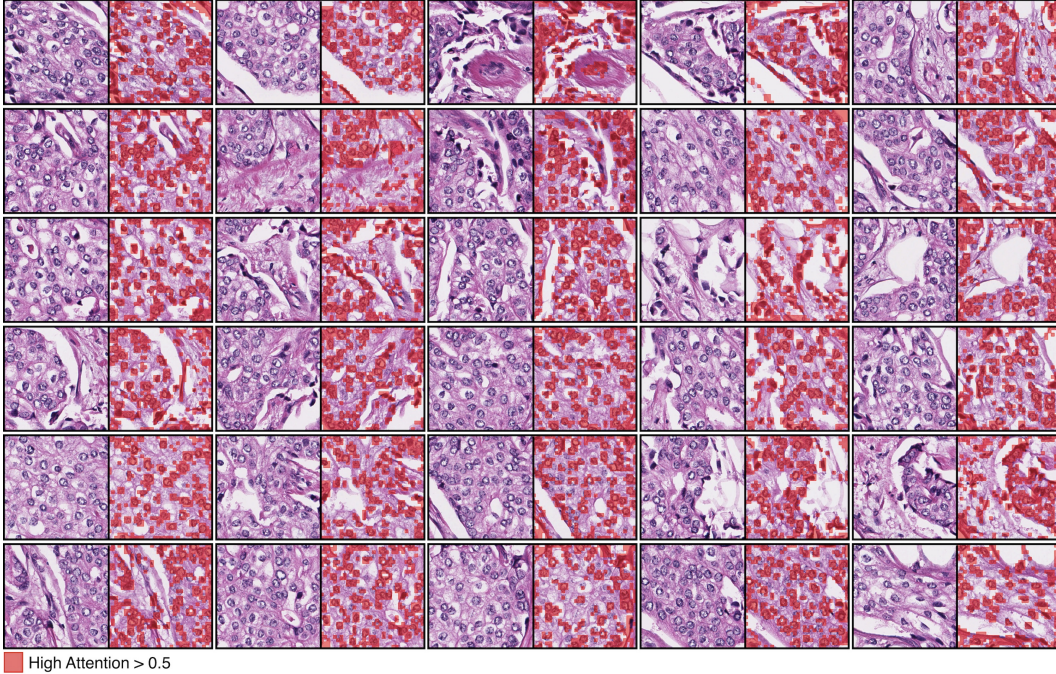
Figure 3: Self-Supervised ViTs localize cells as high-attention visual tokens. We visualize the attention weights for the first attention head, which we empirically found to be robust at localizing cells across a variety of histology image patches. Overlayed in "red" are high-attention 16×16 visual tokens with attention weights greater than 0.5.

5.2 Fine-tuning and evaluating ϕ:

We study a diverse array of tasks on which to assess and compare the different strategies for obtaining patch level embedding ϕ.

Weakly-Supervised Cancer Subtyping: As weakly-supervised evaluation, we used the TCGA-BRCA cohort for Invasive Ductal Carcinoma (IDC) versus Invasive Lobular Carcinoma (ILC) subtyping. Using the CLAM backbone as our set-based network architecture for feature aggregation, we trained CLAM with the following extracted embeddings: 1) ResNet-50-B3, 2) SimCLR, 3) DINO [11]. In addition, we also train all models with different percentage folds of the training dataset ($100\%/75\%/50\%25\%$) as data efficiency experiments. For all models in weakly-supervised evaluation, we report the macro-averaged test AUC performance from 10-fold cross-validation.

Patch-Level Tissue Phenotyping: As tissue phenotyping tasks, we used the following datasets with patch-level annotations:

- **CRC-100K:** CRC-100K is a dataset of 100,000 histological images of human colorectal cancer and healthy tissue, extracted as 224×224 patches at $20\times$ magnification, and is annotated with the following non-overlapping tissue classes: adipose (Adi), background (Back), debris (Deb), lymphocytes (Lym), mucus (Muc), smooth muscle (Mus), normal colon mucosa (Norm), cancer-associated stroma (Str), colorectal adenocarcinoma epithelium (Tum) [2]. We experiment on CRC-100K with and without Macenko stain normalization (SN). As evaluation, we report one-versus-all AUC performance of each class as well as multiclass AUC performance.

- **BreastPathQ:** BreastPathQ is a challenge dataset from the TCGA-BRCA cohort that measures tumor cellularity, which measures the fractional occupancy of tumor cell presence in the image patch [45]. We evaluate on the public train/validation split of the challenge, which provides 2579 and 187 patches respectively at $20\times$, and report mean-squared error (MSE) and Kendall-Tau concordance.

6

Method	Arch	BRCA Subtyping			
		100% Training	75% Training	50% Training	25% Training
IN Transfer	ResNet-50	0.884 ± 0.059	0.850 ± 0.069	0.835 ± 0.087	0.756 ± 0.081
SimCLR	ResNet-50	0.879 ± 0.069	$\mathbf{0.859 \pm 0.079}$	0.820 ± 0.102	0.774 ± 0.094
DINO	ViT	$\mathbf{0.886 \pm 0.059}$	0.852 ± 0.049	$\mathbf{0.862 \pm 0.052}$	$\mathbf{0.809 \pm 0.034}$

Table 1: Comparative study assessing AUC performance of IDC versus ILC subtyping using different self-supervised pretraining methods with varying percentage folds of training data in a 10-fold CV.

Method	SN	Colorectal Tissue Phenotyping								
		Adi	Back	Deb	Lym	Muc	Norm	Str	Tum	All
IN Transfer	Y	0.983	**1.000**	0.997	0.974	0.963	**0.988**	0.982	**0.978**	0.983
SimCLR	Y	0.988	**1.000**	0.994	0.980	0.969	0.973	0.979	0.969	0.981
DINO	Y	**0.999**	**1.000**	**0.999**	**0.985**	**0.992**	0.960	**0.992**	0.967	**0.987**
IN Transfer	N	0.988	**0.909**	0.900	0.870	0.886	**0.988**	0.963	**0.978**	0.935
SimCLR	N	0.981	0.765	0.955	**0.951**	0.926	0.976	0.979	0.973	0.938
DINO	N	**0.991**	0.729	**0.961**	0.950	**0.978**	0.957	**0.990**	0.973	**0.941**

Table 2: Comparative study assessing AUC performance of self-supervised pretraining on CRC-100K with Macenko stain normalization (SN) (**top**) and without SN (**bottom**).

For all patch-level tasks, we trained K-Nearest Neighbors (KNN) on the extracted embeddings of each pretrained model on each dataset. Though SimCLR and DINO were not pretrained using colorectal tissue, CRC-100K was still included in our study design due to exhibiting distinct morphological phenotypes.

5.3 Results

ImageNet features are a strong baseline. Across different tasks, when comparing self-supervised methods against our ResNet-50-B3$_{IN}$ baseline, we find that ImageNet features achieve slightly lower (but comparable) performance on many tasks. In weakly-supervised learning, ResNet-50-B3$_{IN}$ achieves an AUC performance of 0.884 on BRCA subtyping, in comparison to the SIMCLR and DINO which achieved 0.879 and 0.886 AUC respectively (**Table 1**). On patch-level datasets with distinct morphological phenotypes such as CRC-100K (with Macenko normalization), ResNet-50-B3$_{IN}$ achieves a high AUC of 0.983 (**Table 2**). One hypothesis for the surprisingly robust ResNet-50$_{B3, IN}$ performance is that feature maps before the last residual block are low-level feature descriptors, and thus able to distinguish between clearly distinct morphologies such as tumor versus stroma, or tumor versus adipose tissue. Overall, we find that the gap between self-supervised learning and ImageNet transfer learning is smaller than previously found in other studies. However, performance benefit of self-supervised learning may vary depending on organ type (only breast tissue tested) and weakly-supervised architecture (only CLAM tested).

Self-supervised features are robust and sample-efficient. In training weakly-supervised models on less data, we find that self-supervised methods are more robust, as demonstrated in DINO achieving 0.809 AUC with only 25% of the original training data in BRCA subtyping. In comparison, AUC performance using ResNet-50-B3$_{IN}$ degrades to 0.756 (**Table 1**). In patch-level evaluation on more difficult tasks, the performance gap between ResNet-50-B3$_{IN}$ and self-supervised methods is much wider. On CRC-100K without Macenko stain normalization, the macro-averaged AUC for ResNet-50-B3$_{IN}$ decreases to 0.935 in comparison to 0.941 from DINO (**Table 2**). In visualizing UMAP scatter plots of pre-extracted ResNet-50$_{B3, IN}$ features, despite the high AUC performance on both CRC-100K datasets, the representation quality is poor as global structures within the same class types are not preserved (**Figure 4**). On the other hand, global structures for classes such as stroma, tumor, normal, and mucous tissue are well-preserved for self-supervised models. On BreastPathQ, DINO outperforms ResNet-50$_{B3, IN}$ on MSE and Kendall-Tau concordance scores with larger performance gaps of 0.029 versus 0.058 MSE and 0.854 versus 0.824 concordance respectively (**Table 3**).

DINO improves over SimCLR. In comparison with SimCLR used in our ablation study, we observe that DINO also outperforms SimCLR in weakly-supervised tasks (with higher AUC with less
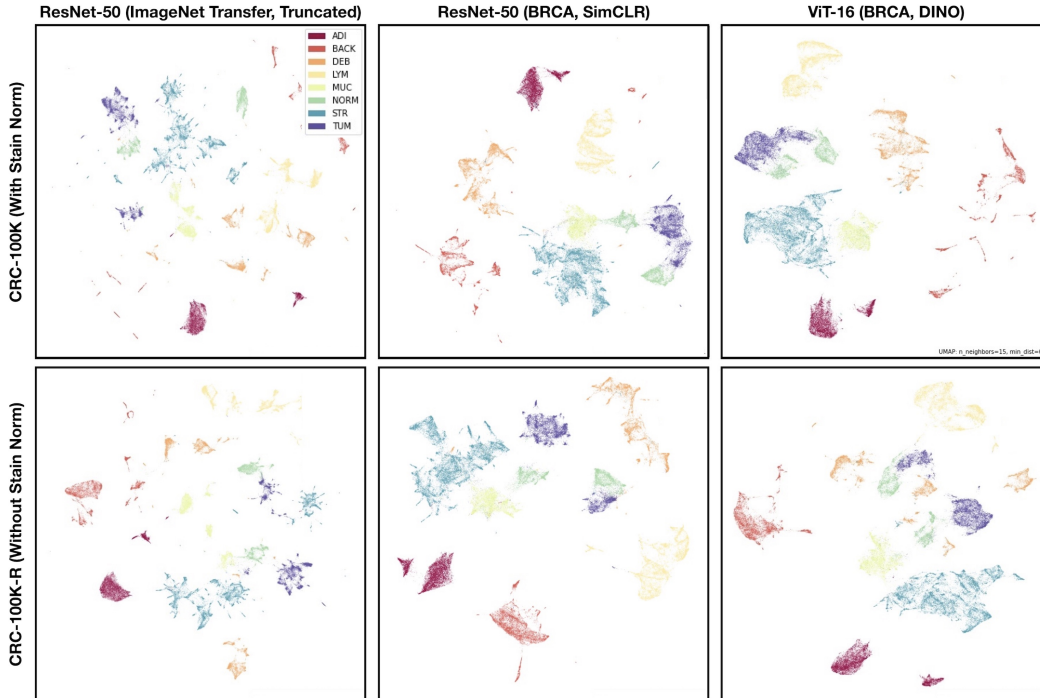
Figure 4: 2D UMAP scatter plot visualizing global structure of extracted feature embeddings of ResNet-50-B3$_{IN}$, SimCLR, and DINO on CRC-100K. For stroma, tumor, and background tissue classes, DINO is able to preserve the global structure of these phenotypes in comparison to ResNet-50-B3$_{IN}$. We used default UMAP parameters of: $neighbors = 15, dist = 0.1$.

finetuning) as well as all patch-level tasks (except lymphocyte classification in CRC-100K without Macenko normalization). In training SimCLR and DINO on the same dataset for pretraining (with default training recipes) and evaluation at 100 epochs, our results suggest that self-supervised learning paradigms such as student-teacher knowledge distillation outperform contrastive-based methods, as constructing positive-negative pairs are not needed in steering representation learning in pathology data.

Method	Tumor Cellularity Prediction	
	MSE $\downarrow$	Kendall-Tau $\uparrow$
IN Transfer	0.058	0.828
SimCLR	0.078	0.788
DINO	**0.029**	**0.854**

Table 3: Comparative study assessing MSE and Kendall-Tau concordance score on BreastPathQ.

DINO learns morphological visual concepts. To introspect into what DINO has learned, we visualize the different attention heads in multi-head self-attention which characterize a normalized distribution over the patch embeddings. Specifically, for a small ViT model in DINO with $n = 6$ heads computed on a 256-length sequence of 384-dim patch embeddings, each attention head computes self-attention on different 64-dim segments of the patch embeddings in the sequence. For each head, we use the attention weights from the [CLS] token that pools over the patch embeddings (which focus on different 64-dim segments), which we overlay on the image patch. In visualizing the overlayed attention weights at the last self-attention block (with weights thresholded at 0.5), we note that visualizations of attention distributions each capture distinct morphological phenotypes, localizing cell location, stroma tissue, and fat / air pockets (**Figure 2, 4**). This observation is in line with current studies that have introspected self-supervised ViT models, in which attention heads can be used as a method for object localization or object discovery in the part-whole hierarchy [22, 46]. In the application of histopathology, this introspection reveals that the embeddings learned for the 16×16 patches capture fine-grained morphological features such as cells and background tissue; we believe this can have applications in the development of automated, interpretable biomarkers.

6   Conclusion

As the field migrates towards difficult phenotyping tasks such as biomarker discovery, more domain-specific encoders are needed in elucidating novel morphological biomarkers not currently identified by human pathologists. In this work, we present a comprehensive empirical evaluation of self-supervised pre-training across a diverse variety of weakly-supervised and patch-level tasks. Future work would further assess the utility of self-supervised methods for learning representations of histopathological images from rare diseases for which there is a natural data paucity of slide-level and patch-level annotations.

7   Acknowledgements

References

[1] Joseph A Ludwig and John N Weinstein. Biomarkers in cancer staging, prognosis and treatment selection. *Nature Reviews Cancer*, 5(11):845–856, 2005.

[2] Jakob Nikolas Kather, Cleo-Aron Weis, Francesco Bianconi, Susanne M Melchers, Lothar R Schad, Timo Gaiser, Alexander Marx, and Frank Gerrit Zöllner. Multi-class texture analysis in colorectal cancer histology. *Scientific reports*, 6(1):1–11, 2016.

[3] Sajid Javed, Arif Mahmood, Muhammad Moazam Fraz, Navid Alemi Koohbanani, Ksenija Benes, Yee-Wah Tsang, Katherine Hewitt, David Epstein, David Snead, and Nasir Rajpoot. Cellular community detection for tissue phenotyping in colorectal cancer histology images. *Medical image analysis*, 63:101696, 2020.

[4] Mahul B Amin, Frederick L Greene, Stephen B Edge, Carolyn C Compton, Jeffrey E Gershenwald, Robert K Brookland, Laura Meyer, Donna M Gress, David R Byrd, and David P Winchester. The eighth edition ajcc cancer staging manual: continuing to build a bridge from a population-based to a more "personalized" approach to cancer staging. *CA: a cancer journal for clinicians*, 67(2):93–99, 2017.

[5] AG Nicholson, LJ Perry, PM Cury, P Jackson, CM McCormick, B Corrin, and AU Wells. Reproducibility of the who/iaslc grading system for pre-invasive squamous lesions of the bronchus: a study of inter-observer and intra-observer variation. *Histopathology*, 38(3):202–208, 2001.

[6] Kimmie Rabe, Olivia L Snir, Veerle Bossuyt, Malini Harigopal, Romulo Celli, and Emily S Reisenbichler. Interobserver variability in breast carcinoma grading results in prognostic stage differences. *Human pathology*, 94:51–57, 2019.

[7] Grant D Carlson, Christina B Calvanese, Hillel Kahane, and Jonathan I Epstein. Accuracy of biopsy gleason scores from a large uropathology laboratory: use of a diagnostic protocol to minimize observer variability. *Urology*, 51(4):525–529, 1998.

[8] Giacomo Novara, Guido Martignoni, Walter Artibani, and Vincenzo Ficarra. Grading systems in renal cell carcinoma. *The Journal of urology*, 177(2):430–436, 2007.

[9] Gabriele Campanella, Matthew G Hanna, Luke Geneslaw, Allen Miraflor, Vitor Werneck Krauss Silva, Klaus J Busam, Edi Brogi, Victor E Reuter, David S Klimstra, and Thomas J Fuchs. Clinical-grade computational pathology using weakly supervised deep learning on whole slide images. *Nature Medicine*, 25(8):1301–1309, 2019.

[10] Ming Y Lu, Richard J Chen, Jingwen Wang, Debora Dillon, and Faisal Mahmood. Semi-supervised histology classification using deep multiple instance learning and contrastive predictive coding. *Advances in Neural Information Processing Systems (NeurIPS) Workshop in Machine Learning for Health*, 2019.

[11] Ming Y Lu, Drew FK Williamson, Tiffany Y Chen, Richard J Chen, Matteo Barbieri, and Faisal Mahmood. Data efficient and weakly supervised computational pathology on whole slide images. *Nature Biomedical Engineering*, 2020.

[12] Ilya Tolstikhin, Neil Houlsby, Alexander Kolesnikov, Lucas Beyer, Xiaohua Zhai, Thomas Unterthiner, Jessica Yung, Daniel Keysers, Jakob Uszkoreit, Mario Lucic, et al. Mlp-mixer: An all-mlp architecture for vision. *arXiv preprint arXiv:2105.01601*, 2021.

[13] Ashish Vaswani, Noam Shazeer, Niki Parmar, Jakob Uszkoreit, Llion Jones, Aidan N Gomez, Lukasz Kaiser, and Illia Polosukhin. Attention is all you need. *arXiv preprint arXiv:1706.03762*, 2017.

[14] Richard J Chen, Ming Y Lu, Muhammad Shaban, Chengkuan Chen, Tiffany Y Chen, Drew FK Williamson, and Faisal Mahmood. Whole slide images are 2d point clouds: Context-aware survival prediction using patch-based graph convolutional networks. In *International Conference on Medical Image Computing and Computer-Assisted Intervention*, pages 339–349. Springer, 2021.

[15] Richard J Chen, Ming Y Lu, Wei-Hung Weng, Tiffany Y Chen, Drew FK Williamson, Trevor Manz, Maha Shady, and Faisal Mahmood. Multimodal co-attention transformer for survival prediction in gigapixel whole slide images. In *Proceedings of the IEEE/CVF International Conference on Computer Vision*, pages 4015–4025, 2021.

[16] Aaron van den Oord, Yazhe Li, and Oriol Vinyals. Representation learning with contrastive predictive coding. *arXiv preprint arXiv:1807.03748*, 2018.

[17] Jeff Donahue and Karen Simonyan. Large scale adversarial representation learning. *arXiv preprint arXiv:1907.02544*, 2019.

[18] Ting Chen, Simon Kornblith, Mohammad Norouzi, and Geoffrey Hinton. A simple framework for contrastive learning of visual representations. In *International conference on machine learning*, pages 1597–1607. PMLR, 2020.

[19] Kaiming He, Haoqi Fan, Yuxin Wu, Saining Xie, and Ross Girshick. Momentum contrast for unsupervised visual representation learning. In *Proceedings of the IEEE/CVF Conference on Computer Vision and Pattern Recognition*, pages 9729–9738, 2020.

[20] Jean-Bastien Grill, Florian Strub, Florent Altché, Corentin Tallec, Pierre H Richemond, Elena Buchatskaya, Carl Doersch, Bernardo Avila Pires, Zhaohan Daniel Guo, Mohammad Gheshlaghi Azar, et al. Bootstrap your own latent: A new approach to self-supervised learning. *arXiv preprint arXiv:2006.07733*, 2020.

[21] Xinlei Chen and Kaiming He. Exploring simple siamese representation learning. In *Proceedings of the IEEE/CVF Conference on Computer Vision and Pattern Recognition*, pages 15750–15758, 2021.

[22] Mathilde Caron, Hugo Touvron, Ishan Misra, Hervé Jégou, Julien Mairal, Piotr Bojanowski, and Armand Joulin. Emerging properties in self-supervised vision transformers. *arXiv preprint arXiv:2104.14294*, 2021.

[23] Jia Deng, Wei Dong, Richard Socher, Li-Jia Li, Kai Li, and Li Fei-Fei. Imagenet: A large-scale hierarchical image database. In *2009 IEEE conference on computer vision and pattern recognition*, pages 248–255. Ieee, 2009.

[24] Kaiming He, Xiangyu Zhang, Shaoqing Ren, and Jian Sun. Deep residual learning for image recognition. In *Proceedings of the IEEE conference on computer vision and pattern recognition*, pages 770–778, 2016.

[25] Jingwen Wang, Richard J Chen, Ming Y Lu, Alexander Baras, and Faisal Mahmood. Weakly supervised prostate tma classification via graph convolutional networks. In *2020 IEEE 17th International Symposium on Biomedical Imaging (ISBI)*, pages 239–243. IEEE, 2020.

[26] Richard J Chen, Ming Y Lu, Jingwen Wang, Drew FK Williamson, Scott J Rodig, Neal I Lindeman, and Faisal Mahmood. Pathomic fusion: an integrated framework for fusing histopathology and genomic features for cancer diagnosis and prognosis. *IEEE Transactions on Medical Imaging*, 2020.

[27] Olivier Dehaene, Axel Camara, Olivier Moindrot, Axel de Lavergne, and Pierre Courtiol. Self-supervision closes the gap between weak and strong supervision in histology. *arXiv preprint arXiv:2012.03583*, 2020.

[28] Yu Zhao, Fan Yang, Yuqi Fang, Hailing Liu, Niyun Zhou, Jun Zhang, Jiarui Sun, Sen Yang, Bjoern Menze, Xinjuan Fan, et al. Predicting lymph node metastasis using histopathological images based on multiple instance learning with deep graph convolution. In *Proceedings of the IEEE/CVF Conference on Computer Vision and Pattern Recognition*, pages 4837–4846, 2020.

[29] Ozan Ciga, Anne L Martel, and Tony Xu. Self supervised contrastive learning for digital histopathology. *arXiv preprint arXiv:2011.13971*, 2020.

[30] Bin Li, Yin Li, and Kevin W Eliceiri. Dual-stream multiple instance learning network for whole slide image classification with self-supervised contrastive learning. In *Proceedings of the IEEE/CVF Conference on Computer Vision and Pattern Recognition*, pages 14318–14328, 2021.

[31] Navid Alemi Koohbanani, Balagopal Unnikrishnan, Syed Ali Khurram, Pavitra Krishnaswamy, and Nasir Rajpoot. Self-path: Self-supervision for classification of pathology images with limited annotations. *IEEE Transactions on Medical Imaging*, 2021.

[32] Ozan Ciga, Tony Xu, and Anne L Martel. Resource and data efficient self supervised learning. *arXiv preprint arXiv:2109.01721*, 2021.

[33] Charlie Saillard, Olivier Dehaene, Tanguy Marchand, Olivier Moindrot, Aurélie Kamoun, Benoit Schmauch, and Simon Jegou. Self supervised learning improves dmmr/msi detection from histology slides across multiple cancers. *arXiv preprint arXiv:2109.05819*, 2021.

[34] Adalberto Claudio Quiros, Nicolas Coudray, Anna Yeaton, Wisuwat Sunhem, Roderick Murray-Smith, Aristotelis Tsirigos, and Ke Yuan. Adversarial learning of cancer tissue representations. In *International Conference on Medical Image Computing and Computer-Assisted Intervention*, pages 602–612. Springer, 2021.

[35] Chetan L Srinidhi, Seung Wook Kim, Fu-Der Chen, and Anne L Martel. Self-supervised driven consistency training for annotation efficient histopathology image analysis. *Medical Image Analysis*, 75:102256, 2022.

[36] Ching-Yao Chuang, Joshua Robinson, Lin Yen-Chen, Antonio Torralba, and Stefanie Jegelka. Debiased contrastive learning. *arXiv preprint arXiv:2007.00224*, 2020.

[37] Xiyue Wang, Sen Yang, Jun Zhang, Minghui Wang, Jing Zhang, Junzhou Huang, Wei Yang, and Xiao Han. Transpath: Transformer-based self-supervised learning for histopathological image classification. In *International Conference on Medical Image Computing and Computer-Assisted Intervention*, pages 186–195. Springer, 2021.

[38] Harrison Edwards and Amos Storkey. Towards a neural statistician. *arXiv preprint arXiv:1606.02185*, 2016.

[39] Manzil Zaheer, Satwik Kottur, Siamak Ravanbakhsh, Barnabas Poczos, Ruslan Salakhutdinov, and Alexander Smola. Deep sets. *Advances in Neural Information Processing Systems*, 2017.

[40] Maximilian Ilse, Jakub Tomczak, and Max Welling. Attention-based deep multiple instance learning. In *Proceedings of the 35th International Conference on Machine Learning*, pages 2132–2141, 2018.

[41] Mohamed Amgad, Habiba Elfandy, Hagar Hussein, Lamees A Atteya, Mai AT Elsebaie, Lamia S Abo El-nasr, Rokia A Sakr, Hazem SE Salem, Ahmed F Ismail, Anas M Saad, et al. Structured crowdsourcing enables convolutional segmentation of histology images. *Bioinformatics*, 35(18):3461–3467, 2019.

[42] Geoffrey E Hinton. Representing part-whole hierarchies in connectionist networks. In *Proceedings of the Tenth Annual Conference of the Cognitive Science Society*, pages 48–54, 1988.

[43] Hang Chang, Alexander Borowsky, Paul Spellman, and Bahram Parvin. Classification of tumor histology via morphometric context. In *Proceedings of the IEEE Conference on Computer Vision and Pattern Recognition*, pages 2203–2210, 2013.

[44] Joel Saltz, Rajarsi Gupta, Le Hou, Tahsin Kurc, Pankaj Singh, Vu Nguyen, Dimitris Samaras, Kenneth R Shroyer, Tianhao Zhao, Rebecca Batiste, et al. Spatial organization and molecular correlation of tumor-infiltrating lymphocytes using deep learning on pathology images. *Cell reports*, 23(1):181–193, 2018.

[45] Nicholas Petrick, Shazia Akbar, Kenny H Cha, Sharon Nofech-Mozes, Berkman Sahiner, Marios A Gavrielides, Jayashree Kalpathy-Cramer, Karen Drukker, Anne L Martel, et al. Spie-aapm-nci breastpathq challenge: an image analysis challenge for quantitative tumor cellularity assessment in breast cancer histology images following neoadjuvant treatment. *Journal of Medical Imaging*, 8(3):034501, 2021.

[46] Oriane Siméoni, Gilles Puy, Huy V Vo, Simon Roburin, Spyros Gidaris, Andrei Bursuc, Patrick Pérez, Renaud Marlet, and Jean Ponce. Localizing objects with self-supervised transformers and no labels. *arXiv preprint arXiv:2109.14279*, 2021.